Nanoscale

Accepted Manuscript

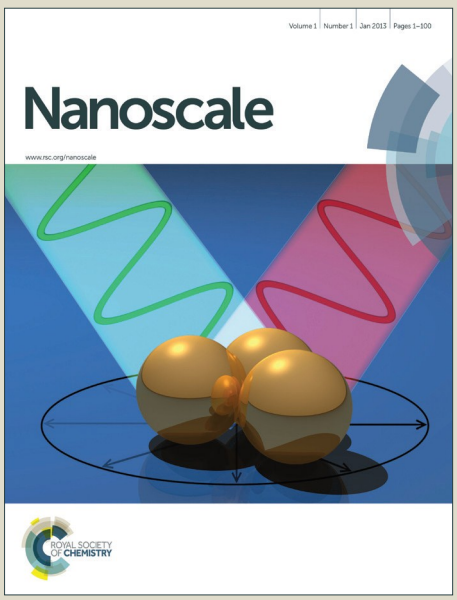

ROYAL SOCIETY OF CHEMISTRY

www.rsc.org/nanoscale

Controlled Synthesis and Magnetic Properties of Iron-Cobalt-Phosphides Nanorods

Weiwei Yang,[1,2] Xiaoming Wu,[2] Yongsheng Yu,[1,2]* Chunhui Yang,[2] Shichong Xu[3] and Haibo Li[3]

[1] State Key Laboratory of Urban Water Resource and Environment, Harbin Institute of Technology, Harbin 150090, China

[2] MIIT Key Laboratory of Critical Materials Technology for New Energy Conversion and Storage, School of Chemistry and Chemical Engineering, Harbin Institute of Technology, Harbin, Heilongjiang 150001, China

[3] Key Laboratory of Functional Materials Physics and Chemistry of the Ministry of Education, Jilin Normal University, Changchun 130103, China

Corresponding Authors *E-mail: ysyu@hit.edu.cn

Abstract

A simple one-step solution-phase synthesis of iron-cobalt-phosphides ($(Fe_{1-x}Co_x)_2P$) nanorods (NRs) was reported in this paper. Through the control of the amount of Co in the samples, the crystal structure of $(Fe_{1-x}Co_x)_2P$ NRs change from pure Fe-rich hexagonal Fe_2P type structure to the mixture of Fe-rich hexagonal Fe_2P and Co-rich orthorhombic Co_2P type structure. These samples show superparamagnetic behavior at room temperature and ferromagnetic properties at 10 K. When the Co composition is 0.09, the $(Fe_{0.91}Co_{0.09})_2P$ sample has the highest coercivity around 5.74 kOe at 10 K. The current route provides a new and general chemical method for tunable preparation of $(Fe_{1-x}Co_x)_2P$ ($x<0.28$) NRs, which are significant for the development of new iron- or cobalt-rich permanent magnet materials without rare-earth or noble metal.

Introduction

Synthesis of ferromagnetic nanoparticle (NP) is key to future fabrication of permanent magnet materials with high energy product.[1-5] Recent studies indicate that tetragonal FePt,[6-9] NdFeB,[10] and hexagonal SmCo[11-13] based alloy NPs are ideal building blocks for fabricating permanent magnets and for studying nanomagnetism due to the strong ferromagnetism observed within their unique structure. However, hard magnetic FePt NPs prepared from solution phase syntheses tend to be superparamagnetic and require high temperature annealing to convert their superparamagnetism to strong ferromagnetism, which often cause NP aggregation or even sintering.[14] Rare-earth metal based alloy NPs of SmCo and NdFeB are extremely difficult to prepare and stabilize due to the easy oxidation of Sm(0) and Nd(0) in the alloy structures. These, plus the limited supply of Pt, Sm and Nd, have motivated the search for Pt-, Sm-, and Nd-alternative magnets. Therefore, the development of new iron- or cobalt-rich permanent magnet materials without rare-earth or noble metal is

of paramount importance in materials science and technology.[15-18]

The transition metal phosphides in bulk are of great interest for a few decades due to their unique properties. Compared with bulk materials, nanocrystalline transition metal phosphides are more attractive candidates for advanced catalytic, electronic, and magnetic applications.[19-28] Furthermore, the studies of their size-dependent physical properties show notable differences between bulk and nanoscale materials. Thus, it is important to develop rational synthetic approaches that yield nanocrystalline transition metal phosphides with careful control over both the composition and the morphology. Recently, binary transition-metal phosphides, Fe_2P, FeP, Co_2P, CoP, Ni_2P, MnP and Rh_2P nanocrystals, have most commonly been prepared by the solution-phase methods in the presence of trioctylphosphine (TOP), metal phosphine complexes, long-chain alkylphosphonic acids, and single-source molecular precursors containing elemental metal and phosphorus.[29-37] Despite these synthetic achievements, the phase or stoichiometry of ternary nanostructured transition-metal phosphides is not well controlled, which have been also rarely explored so far.

In transition-metal phosphides, iron phosphide (Fe_2P) is ferromagnetic phase with a hexagonal crystal structure and a large uniaxial magnetocrystalline anisotropy (K_u = 2.3×10^7erg/cm^3 (at 4.2 K))[38], but its Curie temperature is below room temperature (about 208 K). Cobalt phosphide (Co_2P) is Pauli paramagnetic and has an orthorhombic structure. On the other hand, iron-cobalt-phosphides $(Fe_{1-x}Co_x)_2P$ ($x<0.16$) in bulk, the solid solutions of Fe_2P and Co_2P, are ferromagnetic at room temperature and have a hexagonal crystal structure and large uniaxial magnetocrystalline anisotropy.[39] Haeiwa et al. reported that $(Fe_{0.9}Co_{0.2})_2P$ thin films prepared by the thermal activated reactive evaporation had 1.3 kOe coercivity at room temperature.[40] This work suggests that doping Co in Fe_2P by carefully controlling the Co composition may provide an attractive approach to develop new nanomaterials for magnetic application.

In this paper, we report a simple one-step solution-phase route to synthesize $(Fe_{1-x}Co_x)_2P$ ($x<0.28$) NRs with controlling the Co composition. And the composition-dependent magnetic properties of $(Fe_{1-x}Co_x)_2P$ NRs are studied, exhibiting that $(Fe_{0.91}Co_{0.09})_2P$ NRs show the highest coercivity and the blocking temperature (T_b).

Materials and Methods

Materials

Iron pentacarbonyl ($Fe(CO)_5$, 99.9+% trace metals basis), cobalt(II) acetylacetonate ($Co(acac)_2$) hydrate, trioctylphosphine (technical grade, 90%), hexane (98.5%), ethanol (100%) were all purchased from Sigma Aldrich. The chemicals and solvents were used as received without purification.

Synthesis of $(Fe_{1-x}Co_x)_2P$ NRs

In case $(Fe_{0.91}Co_{0.09})_2P$ NRs, the Fe-TOP complexes solution was prepared by adding 0.25 mL of $Fe(CO)_5$ in 3 mL TOP at 120 ^oC. Then, the resulting reaction mixture was heat to 295 ^oC, and then 4 mL of Co-TOP complex solution prepared by mixing 0.03 g of $Co(acac)_2$ and 4 mL of TOP was added with drop by drop using a syringe within 30 min at 295 ^oC. The solution was maintained at 295 ^oC for 1 h. Then

the heating source was removed, and the solution was cooled to room temperature, after which the solution was exposed to air. A black product was precipitated by adding 40 mL of ethanol, and separated by centrifugation. Finally, the product was dispersed in hexane.

Characterization

X-ray diffraction (XRD) characterization was carried out on a Bruker AXS D8-Advanced diffractometer with Cu K_α radiation (λ =1.5418 Å). The Inductively coupled plasma-atomic emission spectroscopy (ICP-AES) measurements were carried on a JY2000 Ultrace ICP Atomic Emission Spectrometer equipped with a JY AS 421 autosampler and 2400g/mm holographic grating. Samples for transmission electron microscopy (TEM) analysis were prepared by depositing a single drop of diluted NRs dispersion in hexane on amorphous carbon coated copper grids. TEM images were obtained with a Philips CM 20 operating at 200 kV. High-resolution TEM (HRTEM) images and the atomically resolved scanning transmission electron microscopy-EDS (STEM-EDS) images were obtained on a Fei Tecnai Osiris with an accerating votalage of 200 kV. Magnetic studies were carried out using a Quantum Design Superconducting Quantum Interface Device (SQUID) at different temperature.

Results and discussion

$(Fe_{1-x}Co_x)_2P$ (x<0.28) NRs were synthesized by the solution phase thermal decomposition of Fe-TOP and Co-TOP complexes, which were obtained from the reaction of $Fe(CO)_5$ and $Co(acac)_2$ with TOP. The TOP in the reaction mixture not only functions as surfactant and solvent but also as the P sources in the current reaction condition. **Figure 1** shows the typical transmission electron microscopy (TEM) images of the $(Fe_{1-x}Co_x)_2P$ NRs with different amount of Co doping synthesized at 295 °C for 1 h. **Figure 1A** is the TEM image of Fe_2P NRs obtained by directly heating Fe-TOP solution to the reaction temperature, which shows that NPs have diameters of around 4 nm and lengths of up to over 100 nm. By droping the Co-TOP solution at reaction temperature, the diameters of the NRs increase to around 7 nm as shown in **Figure 1B**. Further increasing the amount of Co, the diameters of the NRs do not change (**Figure 1C** and **D**). For the $(Fe_{0.72}Co_{0.28})_2P$ sample, NPs could be also observed beside NRs.

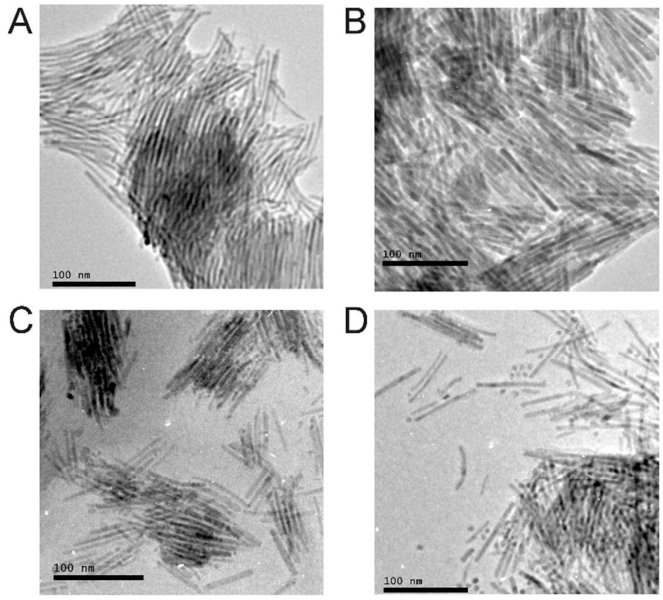

Figure 1. Typical TEM images of (**A**) Fe_2P, (**B**) $(Fe_{0.91}Co_{0.09})_2P$, (**C**) $(Fe_{0.82}Co_{0.18})_2P$ and (**D**) $(Fe_{0.72}Co_{0.28})_2P$ NRs.

The crystal structure of the NRs was characterized by X-ray diffraction (XRD) of the NR assemblies (**Figure 2**). Fe_2P and Co_2P can adopt the hexagonal Fe_2P and orthorhombic Co_2P structure types, which have the strongest peaks around 41°. As shown in **Figure 2**, the XRD patterns of the samples matched the expected line diagram for Fe_2P or Co_2P phase, and no additional diffraction peaks could be observed. And the crystal structure of bulk $(Fe_{1-x}Co_x)_2P$ samples transform from orthorhombic Co_2P type (x>0.16) to hexagonal Fe_2P type (x<0.16).[39] Due to the broad peaks associated with nanoscale crystallite dimensions, it is difficult to distinguish between Fe_2P and Co_2P structure types in these samples and whether Fe-TOP and Co-TOP complex nucleated and grew separately or together.

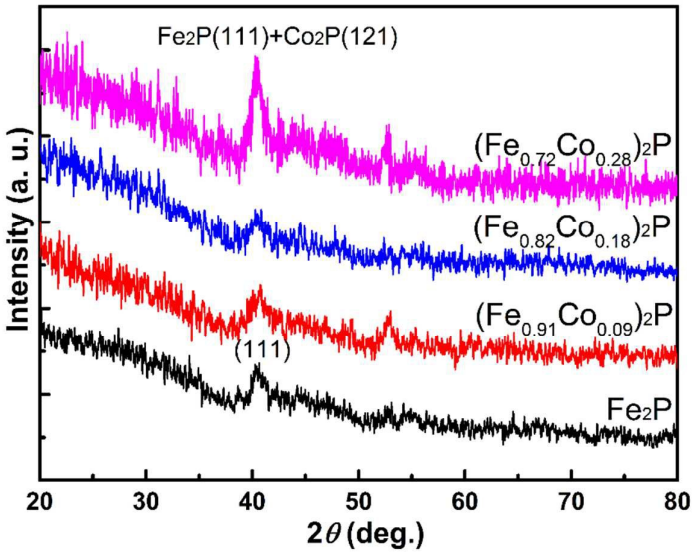

Figure 2. The typical XRD curves of Fe_2P, $(Fe_{0.91}Co_{0.09})_2P$, $(Fe_{0.82}Co_{0.18})_2P$ and $(Fe_{0.72}Co_{0.28})_2P$ NRs.

The TEM image (**Figure 3A)** of a representative NR was taken from $(Fe_{0.92}Co_{0.08})_2P$ samples (shown in Figure 1B). It can be clearly seen that the NR has core/shell structure. The NR is covered with a thin layer shell of amorphous coating. And the core is single crystalline. **Figure 3B** shows the high-resolution TEM (HRTEM) from Figure 3A. We can observe that the lattice fringes are parallel to the NR growth direction. And the interfringe distance was measured to be 0.251 nm, which is close to the lattice spacing of the (200) planes (0.246 nm) in the hexagonal Fe_2P phase, indicating that the (200) planes are parallel to the NR growth direction. These results suggest that TOP could lead to the growth of $(Fe_{0.91}Co_{0.09})_2P$ NR along preferential direction to form one-dimensional nanostructure, because the extra strongly binding TOP surfactants seem to preferentially bind to the crystal growth face due to different crystalline plane energies. In the case of $(Fe_{0.91}Co_{0.09})_2P$ NRs, the direction of the crystal growth was parallel to (200). Since there are two precursors in the reaction solution, it is very important to characterize whether Fe-TOP and Co-TOP complex nucleated and grew separately or together. The corresponding composition distributions in $(Fe_{0.91}Co_{0.09})_2P$ NRs were further characterized by the scanning/transmission electron microscopy-EDS (S/TEM-EDS). **Figure 3C-F** show the elemental mappings of single element Co (yellow), Fe (red), P (green) and the overlapping of the high-angle annular dark field (HAADF) image and the corresponding three elemental mapping in each NR. The color distribution within each NR indicates that each NR contains Co, Fe, P elements, suggesting that Fe-P and Co-P nucleate together and phase segregation is not occurring. It should be noted that, while other compositions were not studied, we expect that $(Fe_{1-x}Co_x)_2P$ samples are similarly homogeneous based upon the bulk-phase diagram.

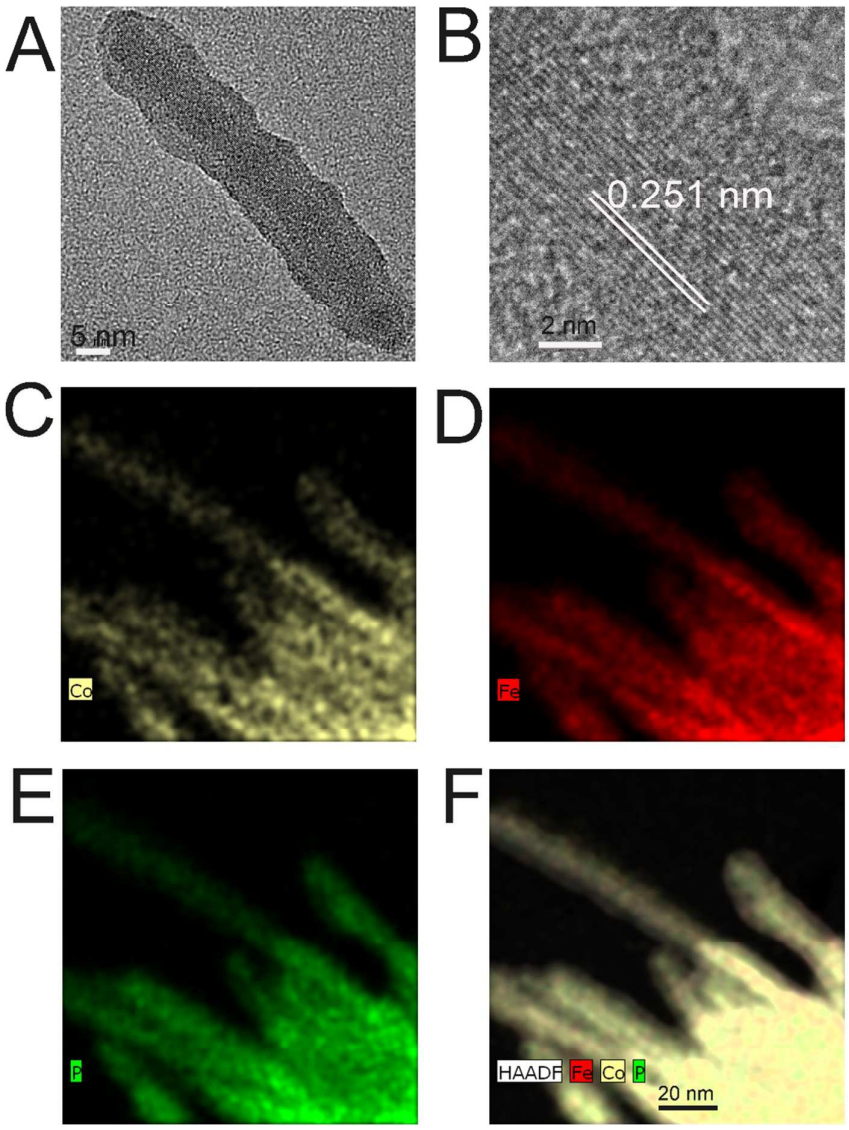

Figure 3. (A) TEM image of single $(Fe_{0.91}Co_{0.09})_2P$ NR from Figure 1B. (B) HRTEM image of a representative NC shown in (**A**). Elemental mappings of (**C**) Co (yellow), (**D**) Fe (red) and (**E**) P (green). (**F**) HADDF image combined the corresponding elemental mapping.

To understand the effect of Co composition on the magnetic properties of the $(Fe_{1-x}Co_x)_2P$ samples, the temperature and field dependences of the magnetic properties of the as-synthesized samples were also measured by using a SQUID at different temperature. All samples are superparamagnetic at 300 K and ferromagnetic at 10 K. For Fe_2P NRs, the coercivity is 3.28 kOe at 10 K. When the Co composition increases to 0.09, the $(Fe_{0.91}Co_{0.09})_2P$ sample has the highest coercivity around 5.74 kOe. By further raising the amount of Co in the sample to 0.18, the coercivity of the $(Fe_{0.82}Co_{0.18})_2P$ sample decreases to 3.58 kOe. When Co composition in the NRs reaches 28%, the coercivity of the $(Fe_{0.72}Co_{0.28})_2P$ sample drops to 0.55 kOe. The

corresponding hysteresis loop shows two-phase behavior. According to the bulk-phase diagram of Fe_2P-Co_2P, the crystal structure of the sample would transform from orthorhombic Co_2P type to hexagonal Fe_2P type for x>0.16. [39] Combined with TEM result (Figure 1D), we conjecture that the NRs in the corresponding TEM image might be Fe-rich hexagonal Fe_2P type structure with high magnetocrystalline anisotropy and the NPs might be Co-rich orthorhombic Co_2P type structure with low magnetocrystalline anisotropy. And the different magnetocrystalline anisotropy of the $(Fe_{0.72}Co_{0.28})_2P$ sample leads to the two-phase behavior in the corresponding hysteresis loop.

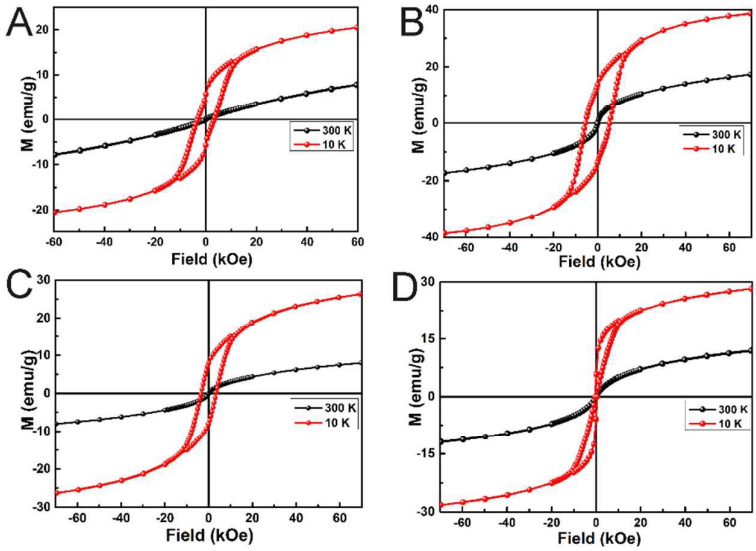

Figure 4. Hysteresis loops of (**A**) Fe_2P, (**B**) $(Fe_{0.91}Co_{0.09})_2P$, (**C**) $(Fe_{0.82}Co_{0.18})_2P$ and (**D**) $(Fe_{0.72}Co_{0.28})_2P$ NRs.

In order to determine the blocking temperature (T_b), the magnetization (M) as a function of temperature (T) for the $(Fe_{1-x}Co_x)_2P$ samples with different Co compositions were measured using zero-field- cooled (ZFC) and field-cooled (FC) measurements at an applied field of 1.0 kOe, as shown in **Figure 5**. The FC *M-T* curves rise monotonically with decreasing temperature, and the ZFC curves exhibit a transformation temperature (T_b) respectively, above which the curve declines monotonically as the temperature rises. Below T_b, the samples change from superparamagnetic to ferromagnetic. T_b of Fe_2P NRs without Co doping is around 80 K. By doping x=0.09 Co, T_b of Fe_2P $(Fe_{0.91}Co_{0.09})_2P$ NRs increases to 170 K. Further increasing Co composition, T_b of the samples decrease. When Co composition in the NRs reaches 0.28, the sample show two transformation temperature at 20 K and between 100 and 200 K, which means that the sample contains two phases with different magnetocrystalline anisotropy. Combined with the measurement of the corresponding hysteresis loop and the bulk-phase diagram, the ZFC/FC measurements also suggest that the $(Fe_{0.72}Co_{0.28})_2P$ sample contains Fe-rich hexagonal Fe_2P and Co-rich orthorhombic Co_2P phases.

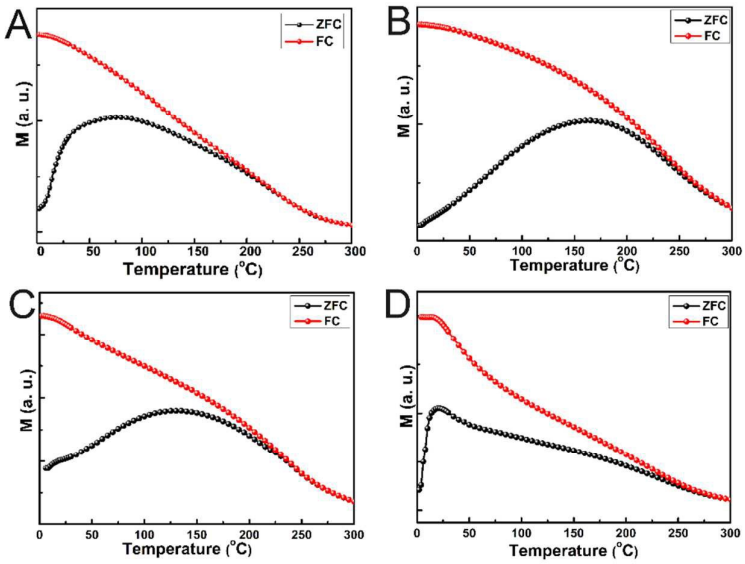

Figure 5. ZFC/FC curves of (**A**) Fe_2P, (**B**) $(Fe_{0.91}Co_{0.09})_2P$, (**C**) $(Fe_{0.82}Co_{0.18})_2P$ and (**D**) $(Fe_{0.72}Co_{0.28})_2P$ NRs. The ZFC curves were obtained by cooling the sample in the absence of an external magnetic field and by measuring the *M* changes over temperature under a field of 1000 Oe. The FC curves were obtained by cooling the sample under a magnetic field of 1000 Oe and then measuring *M* changes over temperature.

Conclusions

In summary, we have reported a simple one-step solution-phase route to prepare $(Fe_{1-x}Co_x)_2P$ (x<0.28) NRs. Through the control of the amount of Co in the samples, the structure of $(Fe_{1-x}Co_x)_2P$ NRs change from pure Fe-rich hexagonal Fe_2P type structure with high magnetocrystalline anisotropy to the mixture of Fe-rich hexagonal Fe_2P and Co-rich orthorhombic Co_2P type structure. These samples show superparamagnetic behavior at room temperature and ferromagnetic properties at 10 K. When the Co composition is 0.09, the $(Fe_{0.91}Co_{0.09})_2P$ sample has the highest coercivity around 5.74 kOe at 10 K. The current route provides a new and general chemical method for tunable preparation of $(Fe_{1-x}Co_x)_2P$ (x<0.28) NRs, which are significant for the development of new iron- or cobalt-rich permanent magnet materials without rare-earth or noble metal.

Acknowledgments

This work was supported by the National Natural Science Foundation of China under Grant (Nos. 51571072, 21305025, 21371071 and 51301075), Open Project of State Key Laboratory of Urban Water Resource and Environment, Harbin Institute of Technology (Grant No QA201611-02), Fundamental Research Funds for the Central Universities (No. AUGA5710012715), Heilongjiang Postdoctoral Scientific Research Development Fund (No. LBH-Q14058) China Postdoctoral Science Foundation (No. 2015M81436), Heilongjiang Postdoctoral Science Foundation (No. LBH-Z15065)

and Research Project of Key Laboratory of Functional Materials Physics and Chemistry of the Ministry of Education (No. 2015001).

References

1. L. Yu, C. Yang, and Y. Hou, Nanoscale, 2014, 6, 10638-10642.
2. F. Liu, J. Zhu, W. Yang, Y. Dong, and Y. Hou, C. Zhang, H. Yin, and S. Sun, Angew. Chem. Int. Edit., 2014, 53, 2176-2180.
3. F. Liu, Y. Dong, W. Yang, J. Yu, Z. Xu, and Y. Hou, Chem. Eur. J., 2014, 20, 15197-15202.
4. F. Liu, Y. Hou, and S. Gao, Chem. Soc. Rev., 2014, 43, 8098-8113.
5. L. Yu, Y. Zhang, W. Yang, J. He, K. Dong and Y. Hou, Nanoscale, DOI: 10.1039/C6NR03172B.
6. J. Kim, C. B. Rong, J. P. Liu, and S.H. Sun, Adv. Mater., 2009, 21, 906-909.
7. J.-M. Qiu, J.-P. Wang, Adv. Mater., 2007, 19. 1703-1706.
8. S. H. Sun, C. B. Murray, D. Weller, L. Folks, A. Moser, Science, 2000, 287, 1989.
9. Y. Yu, P. Mukherjee, Y. Tian, X.-Z. Li, J. E. Shield and D. J. Sellmyer, Nanoscale, 2014,6, 12050-12055
10. W. B. Cui, Y. K. Takahashi , and K. Hono, Adv. Mater., 2012, 24, 6530-6541.
11. Y. L. Hou, Z. C. Xu, S. Peng, C. B. Rong, J. P. Liu, and S. H. Sun, Adv. Mater., 2007, 19, 3349.
12. C. Yang, L. Jia, S. Wang, C. Gao, D. Shi, Y. Hou, and S. Gao, Sci. Rep., 2013, 3, 3542.
13. H. W. Zhang, S. Peng, C. B. Rong, J. P. Liu, Y. Zhang, M. J. Kramer and S. H. Sun, J. Mater. Chem., 2011, 21, 16873-16876.
14. H. Zeng, J. Li, J. P. Liu, Z. L. Wang, S. H. Sun, Nature, 2002, 420, 395-398.
15. M. J. Kramer, R. W. McCallum, I. A. Anderson, S. Constantinides, J. Min. Met. Mat. Soc., 2012, 64, 752-761.
16. Y. S. Yu, A. Mendoza-Garcia, B. Ning, S. H. Sun, Adv. Mater., 2013, 22, 3090-3094.
17. B. Balasubramanian, B. Das, R. Skomski, W.Y. Zhang, and D.J. Sellmyer, Adv. Mater., 2013, 25, 6090-6093.
18. Y. Yu, K. Sun, Y. Tian, X.-Z. Li, M. J. Kramer, D. J. Sellmyer, J. E. Shield, and S. Sun, Nano Lett., 2013, 13, 4975-4979.
19. K. J. De Vos, W. A. J. J. Velge, M. G. Van Der Steeg, and H. Zijlstra, J. Appl. Phys., 1962, 33, 1320-1322.
20. E. Ye, S.-Y. Zhang, S. H. Lim, M. Bosman, Z. Zhang, K. Y. Win, and M.-Y. Han, Chem. Eur. J. 2011, 17, 5982-5988.
21. E. J. Popczun, C. G. Read, C. W. Roske, N. S. Lewis, R. E. Schaak, Angew. Chem. Int. Ed., 2014, 19, 5427-5430.
22. E. J. Popczun, J. R. McKone, C. G. Read, A. J. Biacchi, A. M. Wiltrout, N. S. Lewis, and R. E. Schaak, J. Am. Chem. Soc., 2013, 135, 9267-9270.
23. C.-T. Lo and P.-Y. Kuo, J. Phys. Chem. C, 2010, 114, 4808-4815.
24. E. Muthuswamy, P. Ram Kharel, G. Lawes, and S. L. Brock, ACS Nano, 2009, 3, 2383-2393.
25. K. A. Gregg, S.C. Perera, G. Lawes, S. Shinozaki, and S. L. Brock, Chem. Mater.,

2006, 18, 879-886.
26. J. Park, B. Koo, K. Y. Yoon, Y. Hwang, M. Kang, J.-G. Park, and T. Hyeon, J. Am. Chem. Soc., 2005, 127, 8433-8440.
27. R.-K. Chiang and R.-T. Chiang, Inorg. Chem., 2007, 46, 369-371.
28. J. Wang, Q. Yang, Z. Zhang, and S. Sun, Chem. Eur. J., 2010, 16, 7916-7924.
29. W. Yang, Y. Huang, J. Fan, Y. Yu, C. Yang, and H. Li, Nanoscale., 2016, 8, 4898-902.
30. J.-H. Chen, M.-F. Tai and K.-M. Chi, J. Mater. Chem., 2004, 14, 296-298.
31. C. Qian, F. Kim, L. Ma, F. Tsui, P. Yang, and J. Liu, J. Am. Chem. Soc., 2004, 126, 1195-1198.
32. J. Park, B. Koo, Y. Hwang, C. Bae, K. An, J.-G. Park, H. M. Park and T. Hyeon, Angew. Chem., Int. Ed., 2004, 116, 2332-2335
33. A. E. Henkes and R. E. Schaak, Inorg. Chem., 2008, 4, 671-677.
34. A. E. Henkes, Y. Vasquez , and R. E. Schaak, J. Am. Chem. Soc., 2007, 129, 1896-1897.
35. A. E. Henkes and R. E. Schaak, Chem. Mater., 2007, 19, 4234-4242.
36. A. T. Kelly, I. Rusakova, T. Ould-Ely, C. Hofmann, A. Lüttge, and K. H. Whitmire, Nano Lett., 2007, 7, 2920-2925.
37. S.-Y. Zhang, E. Ye, S. Liu, S. H. Lim, S. Y. Tee, Z. Dong, M.-Y. Han, Adv. Mater., 2012, 24, 4369-4375.
38. T. Hokabe, J. Sci. Hiroshima Univ., Sea. A, 1978, 42, 1-29.
39. R. Fruchart, A. Roger and J. P. Senateur, J. Appl. Phys., 1969, 40, 1250-1257.
40. T. Haeiwa and M. Matsumoto, IEEE Trans. Magn., 1988, 24, 2055-2059.